REFERENCES

Goldsbury R., Richer H. B., Anderson J., Dotter A., Sarajedini A., Woodley K., 2010, AJ, 140, 1830
Vasiliev E., Baumgardt H., 2021, MNRAS, 505, 5978

APPENDIX A: MAMPOSST-PM OUTCOME

Tables with results from the main MAMPOSST-PM fits.

APPENDIX B: EXTRA PLOTS

Plots available as online material.

This paper has been typeset from a TEX/LATEX file prepared by the author.

Table A1. Main results of the MAMPOSSt-PM mass-modelling fit of NGC 3201 and NGC 6397.

Model	Cluster ID	Test	R^{-1}	β_0	$\beta_{\rm out}$	$r_{\rm GC}$ [pc]	$n_{\rm GC}$	$M_{\rm GC}$ [10^5 M$_\odot$]	$r_{\rm CUO}$ [pc]	$M_{\rm CUO}$ [M$_\odot$]	$M_{\rm BH}$ [M$_\odot$]	ΔAICc
(1)	(2)	(3)	(4)	(5)	(6)	(7)	(8)	(9)	(10)	(11)	(12)	(13)
1	NGC 3201	–	0.002	0	0	$5.070^{+0.233}_{-0.273}$	$0.99^{+0.04}_{-0.03}$	$1.55^{+0.07}_{-0.08}$	–	–	–	0.00
2	NGC 3201	–	0.007	0	0	$5.269^{+0.254}_{-0.327}$	$1.01^{+0.04}_{-0.04}$	$1.53^{+0.09}_{-0.06}$	–	–	1144^{+202}_{-935}	-3.53
3	NGC 3201	–	0.004	0	0	$5.378^{+0.130}_{-0.453}$	$1.03^{+0.02}_{-0.06}$	$1.56^{+0.05}_{-0.10}$	$0.153^{+0.087}_{-0.149}$	1217^{+254}_{-1046}	–	-1.65
4	NGC 3201	–	0.005	0	0	$5.283^{+0.258}_{-0.316}$	$1.01^{+0.04}_{-0.04}$	$1.53^{+0.08}_{-0.08}$	$0.122^{+0.265}_{-0.118}$	342^{+697}_{-310}	825^{+230}_{-783}	0.35
5	NGC 3201	$\beta(r)$	0.002	$0.03^{+0.07}_{-0.06}$	$0.02^{+0.13}_{-0.20}$	$5.119^{+0.285}_{-0.307}$	$1.00^{+0.04}_{-0.03}$	$1.56^{+0.08}_{-0.08}$	–	–	–	3.65
6	NGC 3201	$\beta(r)$	0.005	$-0.07^{+0.11}_{-0.06}$	$0.07^{+0.16}_{-0.18}$	$5.341^{+0.284}_{-0.375}$	$1.03^{+0.03}_{-0.05}$	$1.54^{+0.08}_{-0.08}$	–	–	1273^{+378}_{-991}	-0.07
7	NGC 3201	$\beta(r)$	0.006	$-0.02^{+0.07}_{-0.10}$	$0.04^{+0.19}_{-0.15}$	$5.376^{+0.236}_{-0.410}$	$1.01^{+0.04}_{-0.03}$	$1.55^{+0.06}_{-0.09}$	$0.107^{+0.111}_{-0.103}$	1289^{+478}_{-1039}	–	1.76
8	NGC 3201	$\beta(r)$	0.012	$-0.04^{+0.07}_{-0.10}$	$0.05^{+0.18}_{-0.15}$	$5.278^{+0.354}_{-0.288}$	$1.01^{+0.04}_{-0.04}$	$1.50^{+0.11}_{-0.04}$	$0.089^{+0.312}_{-0.084}$	1367^{+0}_{-1334}	138^{+1156}_{-98}	3.85
9	NGC 3201	$(\alpha_0,\,\delta_0)$	0.002	0	0	$5.026^{+0.271}_{-0.237}$	$1.00^{+0.04}_{-0.04}$	$1.54^{+0.08}_{-0.07}$	–	–	–	87009.01
10	NGC 3201	$(\alpha_0,\,\delta_0)$	0.004	0	0	$5.224^{+0.293}_{-0.298}$	$1.01^{+0.04}_{-0.03}$	$1.53^{+0.09}_{-0.07}$	–	–	992^{+385}_{-797}	87005.52
11	NGC 3201	$(\alpha_0,\,\delta_0)$	0.003	0	0	$5.192^{+0.318}_{-0.264}$	$1.02^{+0.03}_{-0.05}$	$1.51^{+0.10}_{-0.05}$	$0.091^{+0.150}_{-0.086}$	1081^{+386}_{-905}	–	87007.14
12	NGC 3201	$(\alpha_0,\,\delta_0)$	0.009	0	0	$5.291^{+0.264}_{-0.325}$	$1.01^{+0.05}_{-0.03}$	$1.54^{+0.08}_{-0.08}$	$0.134^{+0.268}_{-0.129}$	1021^{+21}_{-990}	59^{+1011}_{-18}	87009.26
13	NGC 3201	σ_μ	0.002	0	0	$4.987^{+0.463}_{-0.305}$	$1.00^{+0.05}_{-0.04}$	$1.42^{+0.14}_{-0.09}$	–	–	–	36566.09
14	NGC 3201	σ_μ	0.005	0	0	$5.029^{+0.455}_{-0.320}$	$1.01^{+0.05}_{-0.05}$	$1.41^{+0.15}_{-0.08}$	–	–	320^{+125}_{-298}	36567.18
15	NGC 3201	σ_μ	0.001	0	0	$5.065^{+0.416}_{-0.368}$	$1.02^{+0.04}_{-0.05}$	$1.42^{+0.13}_{-0.10}$	$0.016^{+0.522}_{-0.010}$	323^{+211}_{-298}	–	36569.16
16	NGC 3201	σ_μ	0.004	0	0	$5.081^{+0.426}_{-0.350}$	$1.03^{+0.04}_{-0.05}$	$1.42^{+0.13}_{-0.10}$	$0.116^{+0.498}_{-0.110}$	363^{+67}_{-342}	15^{+351}_{-0}	36571.14
17	NGC 3201	Bulk μ	0.002	0	0	$5.022^{+0.277}_{-0.231}$	$1.00^{+0.04}_{-0.03}$	$1.54^{+0.08}_{-0.07}$	–	–	–	87210.35
18	NGC 3201	Bulk μ	0.004	0	0	$5.290^{+0.206}_{-0.368}$	$1.02^{+0.03}_{-0.04}$	$1.54^{+0.08}_{-0.07}$	–	–	1055^{+236}_{-892}	87207.12
19	NGC 3201	Bulk μ	0.003	0	0	$5.370^{+0.131}_{-0.440}$	$1.03^{+0.03}_{-0.05}$	$1.56^{+0.06}_{-0.09}$	$0.131^{+0.131}_{-0.126}$	1242^{+191}_{-1082}	–	87208.94
20	NGC 3201	Bulk μ	0.008	0	0	$5.245^{+0.278}_{-0.295}$	$1.00^{+0.05}_{-0.03}$	$1.53^{+0.08}_{-0.07}$	$0.118^{+0.286}_{-0.113}$	985^{+58}_{-952}	133^{+825}_{-99}	87210.98

Notes: Columns are (1) Model number; (2) Cluster ID; (3) Test type: "$\beta(r)$" for a free anisotropy model, "$(\alpha_0,\,\delta_0)$" for the test of a different centre (Goldsbury et al. 2010), "σ_μ" for the test with half of the standard error threshold, "Bulk μ" for the test setting the *HST* bulk proper motion as the one from Vasiliev & Baumgardt (2021); (4) MCMC convergence criterion ($R^{-1} \leq 0.02$ is considered as properly converged); (5) anisotropy value at $r = 0$; (6) anisotropy value at the data's most distant projected radius (usually around 10 arcmin); (7) Sérsic projected half mass radius $R_{\rm e}$ (in pc) of the mass density profile of the globular cluster; (8) Sérsic index n of the mass density profile of the globular cluster; (9) Total globular cluster mass (without dark central component), in M$_\odot$; (10) Plummer projected half mass radius $a_{\rm P}$ (in pc) of the mass density profile of the central sub-cluster of unresolved objects (CUO); (11) Total mass of the CUO, in M$_\odot$; (12) Central black hole mass, in M$_\odot$; (13) Difference in AICc (eq. [14]) relative to model 1 for NGC 3201 and to model 23, for NGC 6397. We highlight the maximum likelihood values in *orange* when they were outside the 16-84 percentiles of the posterior distribution, and the convergence criterion R^{-1} in *red* when the MCMC convergence was poor. The uncertainties are from the 16th and 84th percentiles of the marginal distributions. The lines coloured in *lavender* indicate our preferred models for each cluster. We did not consider the AICc diagnosis when the data set was different from the respective standard model.

Table A1 – *continued*

Model	Cluster ID	Test	R^{-1}	β_0	$\beta_{\rm out}$	$r_{\rm GC}$ [pc]	$n_{\rm GC}$	$M_{\rm GC}$ [10^5 M$_\odot$]	$r_{\rm CUO}$ [pc]	$M_{\rm CUO}$ [M$_\odot$]	$M_{\rm BH}$ [M$_\odot$]	ΔAICc
(1)	(2)	(3)	(4)	(5)	(6)	(7)	(8)	(9)	(10)	(11)	(12)	(13)
29	NGC 6397	–	0.008	0	0	$3.150^{+0.514}_{-0.097}$	$3.32^{+0.60}_{-0.04}$	$1.08^{+0.07}_{-0.02}$	–	–	–	0.00
30	NGC 6397	–	0.005	0	0	$3.461^{+0.133}_{-0.169}$	$3.27^{+0.05}_{-0.06}$	$1.12^{+0.03}_{-0.03}$	–	–	578^{+136}_{-174}	-22.98
31	NGC 6397	–	0.005	0	0	$3.544^{+0.116}_{-0.213}$	$3.27^{+0.05}_{-0.06}$	$1.13^{+0.03}_{-0.04}$	$0.041^{+0.007}_{-0.037}$	807^{+123}_{-323}	–	-24.06
32	NGC 6397	–	0.017	0	0	$3.564^{+0.073}_{-0.247}$	$3.29^{+0.03}_{-0.07}$	$1.13^{+0.02}_{-0.04}$	$0.034^{+0.064}_{-0.031}$	749^{+0}_{-703}	21^{+518}_{-0}	-21.91
33	NGC 6397	$\beta(r)$	0.012	$0.06^{+0.03}_{-0.06}$	$-0.01^{+0.07}_{-0.05}$	$3.197^{+0.397}_{-0.124}$	$3.32^{+0.50}_{-0.05}$	$1.09^{+0.05}_{-0.03}$	–	–	–	2.32
34	NGC 6397	$\beta(r)$	0.004	$0.00^{+0.04}_{-0.05}$	$0.08^{+0.03}_{-0.09}$	$3.488^{+0.148}_{-0.171}$	$3.28^{+0.05}_{-0.06}$	$1.12^{+0.03}_{-0.03}$	–	–	598^{+146}_{-183}	-19.27
35	NGC 6397	$\beta(r)$	0.010	$-0.02^{+0.04}_{-0.05}$	$0.07^{+0.05}_{-0.07}$	$3.538^{+0.162}_{-0.179}$	$3.29^{+0.03}_{-0.08}$	$1.12^{+0.03}_{-0.03}$	$0.036^{+0.012}_{-0.032}$	711^{+275}_{-201}	–	-20.57
36	NGC 6397	$\beta(r)$	0.016	$-0.01^{+0.05}_{-0.05}$	$0.07^{+0.04}_{-0.08}$	$3.202^{+0.083}_{-0.236}$	$2.18^{+0.11}_{-0.02}$	$1.07^{+0.01}_{-0.04}$	$0.084^{+0.071}_{-0.031}$	1924^{+301}_{-853}	28^{+462}_{-6}	-14.97
37	NGC 6397	(α_0, δ_0)	0.004	0	0	$3.151^{+0.517}_{-0.098}$	$3.31^{+0.61}_{-0.03}$	$1.08^{+0.07}_{-0.02}$	–	–	–	144066.39
38	NGC 6397	(α_0, δ_0)	0.008	0	0	$3.474^{+0.125}_{-0.180}$	$3.27^{+0.05}_{-0.06}$	$1.12^{+0.03}_{-0.03}$	–	–	590^{+127}_{-183}	144044.21
39	NGC 6397	(α_0, δ_0)	0.010	0	0	$3.525^{+0.141}_{-0.188}$	$3.27^{+0.05}_{-0.06}$	$1.12^{+0.03}_{-0.03}$	$0.033^{+0.017}_{-0.029}$	780^{+168}_{-290}	–	144042.75
40	NGC 6397	(α_0, δ_0)	0.013	0	0	$3.540^{+0.105}_{-0.217}$	$3.28^{+0.04}_{-0.07}$	$1.13^{+0.03}_{-0.04}$	$0.040^{+0.058}_{-0.037}$	759^{+0}_{-713}	42^{+506}_{-13}	144045.05
41	NGC 6397	σ_μ	0.002	0	0	$3.342^{+0.302}_{-0.210}$	$3.93^{+0.22}_{-0.22}$	$1.05^{+0.06}_{-0.04}$	–	–	–	84517.03
42	NGC 6397	σ_μ	0.002	0	0	$3.235^{+0.270}_{-0.141}$	$3.27^{+0.09}_{-0.08}$	$1.05^{+0.06}_{-0.03}$	–	–	569^{+151}_{-195}	84499.35
43	NGC 6397	σ_μ	0.005	0	0	$3.462^{+0.103}_{-0.322}$	$3.26^{+0.08}_{-0.08}$	$1.09^{+0.03}_{-0.07}$	$0.045^{+0.008}_{-0.041}$	851^{+154}_{-372}	–	84497.79
44	NGC 6397	σ_μ	0.046	0	0	$3.420^{+0.133}_{-0.312}$	$3.25^{+0.09}_{-0.07}$	$1.07^{+0.04}_{-0.05}$	$0.052^{+0.061}_{-0.048}$	866^{+0}_{-814}	101^{+434}_{-72}	84500.11
45	NGC 6397	Bulk μ	0.002	0	0	$3.119^{+0.538}_{-0.069}$	$3.31^{+0.61}_{-0.03}$	$1.07^{+0.08}_{-0.02}$	–	–	–	144061.37
46	NGC 6397	Bulk μ	0.001	0	0	$3.448^{+0.140}_{-0.167}$	$3.28^{+0.04}_{-0.07}$	$1.12^{+0.03}_{-0.03}$	–	–	522^{+186}_{-124}	144038.69
47	NGC 6397	Bulk μ	0.008	0	0	$3.526^{+0.108}_{-0.220}$	$3.27^{+0.04}_{-0.06}$	$1.12^{+0.02}_{-0.04}$	$0.037^{+0.010}_{-0.034}$	781^{+133}_{-317}	–	144036.01
48	NGC 6397	Bulk μ	0.006	0	0	$3.502^{+0.137}_{-0.187}$	$3.27^{+0.05}_{-0.05}$	$1.13^{+0.02}_{-0.04}$	$0.030^{+0.074}_{-0.026}$	665^{+53}_{-620}	14^{+530}_{-0}	144039.97

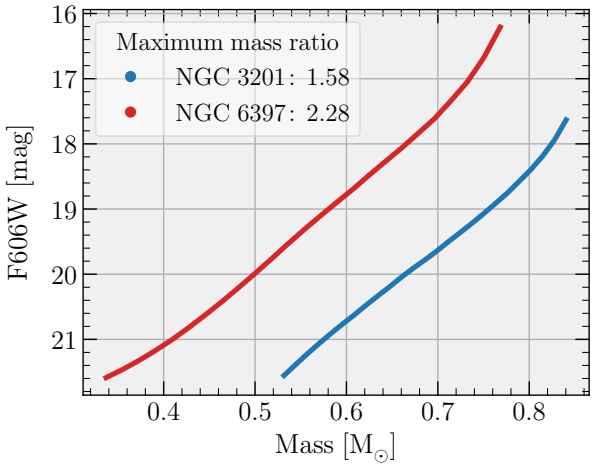

Figure B1. *Mass-magnitude:* Mass-magnitude (F606W) relation from PARSEC isochrones, for NGC 3201 in *blue* and for NGC 6397 in *red*. The limits of the curves represent the respective limits of our cleaned data. The box indicates the ratio $m_{\rm max}/m_{\rm min}$ for the cleaned data.

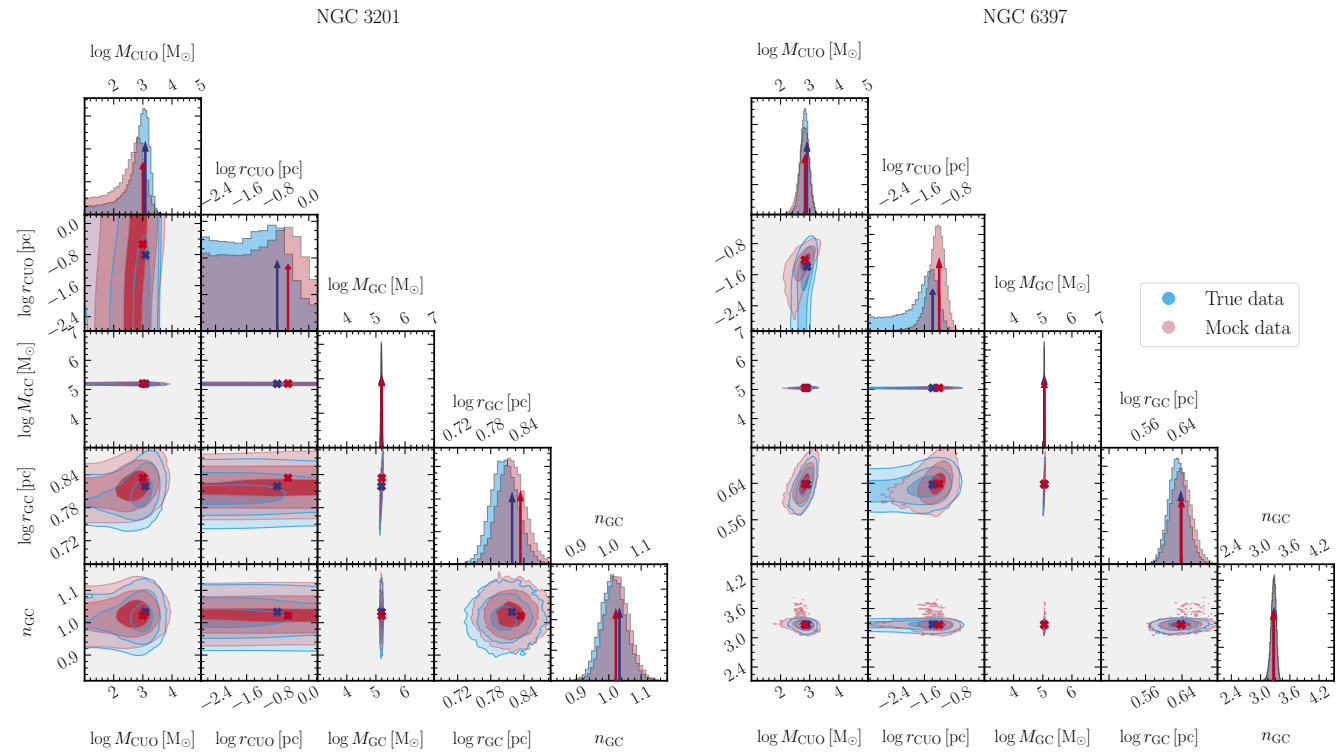

Figure B2. *Corner plots:* MAMPOSSt-PM corner plots of the mass modelling fit of NGC 3201 (**left**) and NGC 6397 (**right**). The free parameters are, from **top** to **bottom**: mass of the sub-cluster of unresolved objects (CUO); Plummer 2D half-mass radius of the CUO; total stellar mass of the cluster; half-projected mass radius $R_{\rm e}$ (in pc) of the GC stellar mass profile and the Sérsic index n of the GC stellar mass profile. Again, the priors are flat for $M_{\rm CUO}$ and $M_{\rm GC}$ within the plotted range and zero outside, while they are Gaussian for the two radii and Sérsic index, centred on the middles of the panels and extending to $\pm 3\,\sigma$ at the edges of the panels, and zero beyond. In *blue*, we indicate the outcome from the fits of the true data (i.e., *HST* and *Gaia* EDR3), while the fits from mock data with a CUO prescription, constructed with Agama (see Section 4.2), are in *red*.

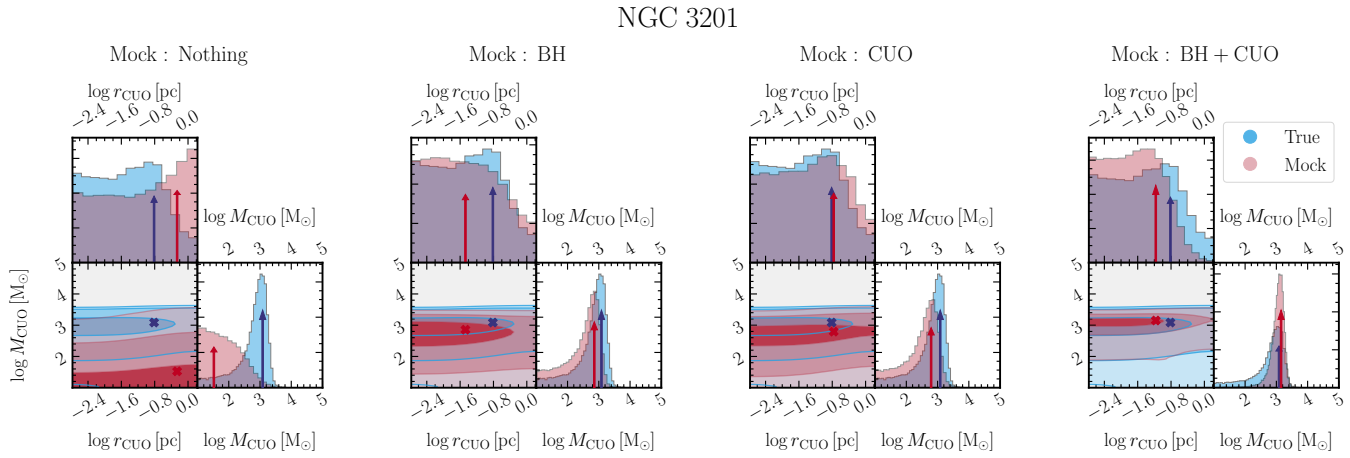

Figure B3. *Mock data with underestimated errors:* Similarly to Figure 4, we present the corner plots of the logarithm of the cluster of unresolved objects (CUO) mass (in M$_\odot$) and 2D Plummer half mass radius (in pc) for the true data (*HST* and *Gaia* EDR3) in *blue* and the mock data (constructed with Agama) in *red*, for NGC 3201, which had different results when performing data cleaning with different error thresholds. The priors are flat for $M_{\rm CUO}$ within the plotted range and zero outside, while they are Gaussian for the scale radii, centred on the middles of the panels and extending to $\pm 3\,\sigma$ at the edges of the panels, and zero beyond. The mock data prescription is, from **left** to **right**: No central dark component (Nothing); a central black hole alone (BH); a central CUO (CUO) and both a central black hole and CUO (BH+CUO). The mocks were constructed with the best values of each respective isotropic mass model from Table A1 (online version), but the errors provided to MAMPOSSt-PM in the inner regions (i.e., up to $2\,r_{\rm CUO}$) were underestimated by 10%, in order to test the effect of underestimated errors in the true data. We notice that no strong mass overestimation, such as the mass peak for models with a central mass, is due to the underestimated errors.

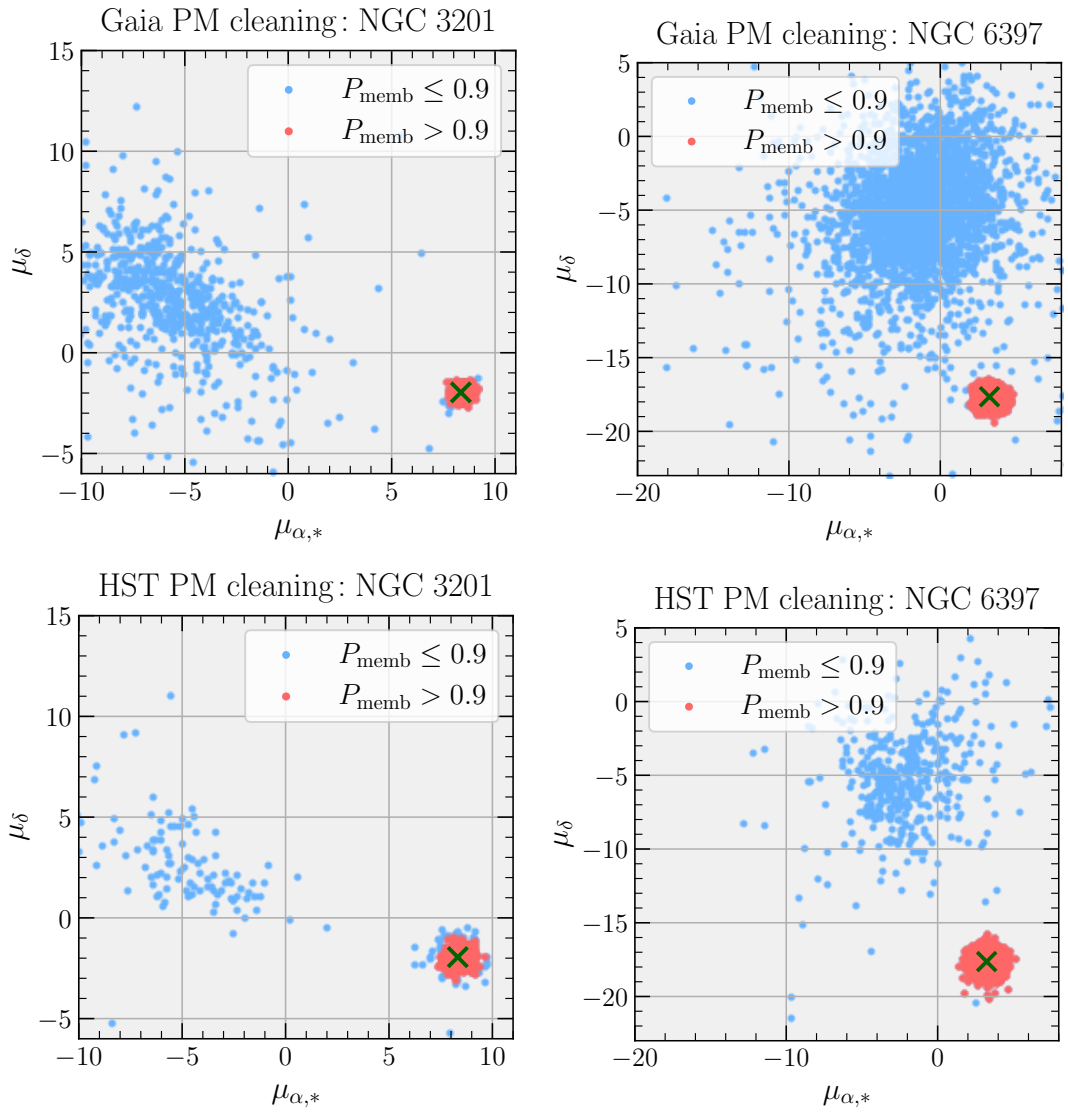

Figure B4. *Proper motion interloper filter:* Comparison between the proper motion subset before (**blue**) and after (**red**) the interloper proper motion cleaning described in Section 3.4. *Upper plots* display the *Gaia* EDR3 proper motion space, while *lower plots* depict the *HST* proper motion space. The stars from NGC 3201 are on the *left* column, while the *right* column shows the NGC 6397 stars. The **green crosses** represent the bulk proper motion of the clusters derived by Vitral (2021) with *Gaia* EDR3.

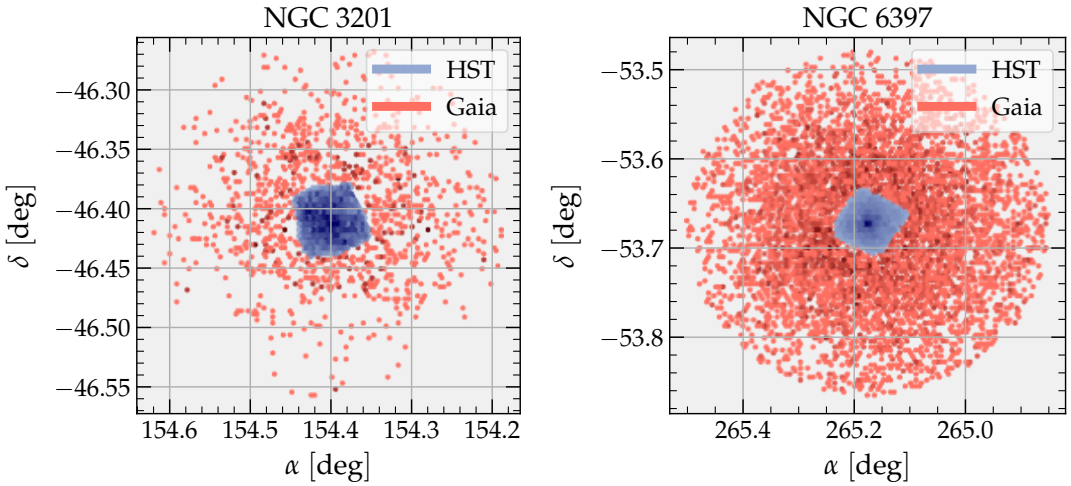

Figure B5. *Sky view:* Position in the sky of the data used in our modelling. Stars associated with *HST* are in *blue*, while the ones associated with *Gaia* EDR3 are in *red*.

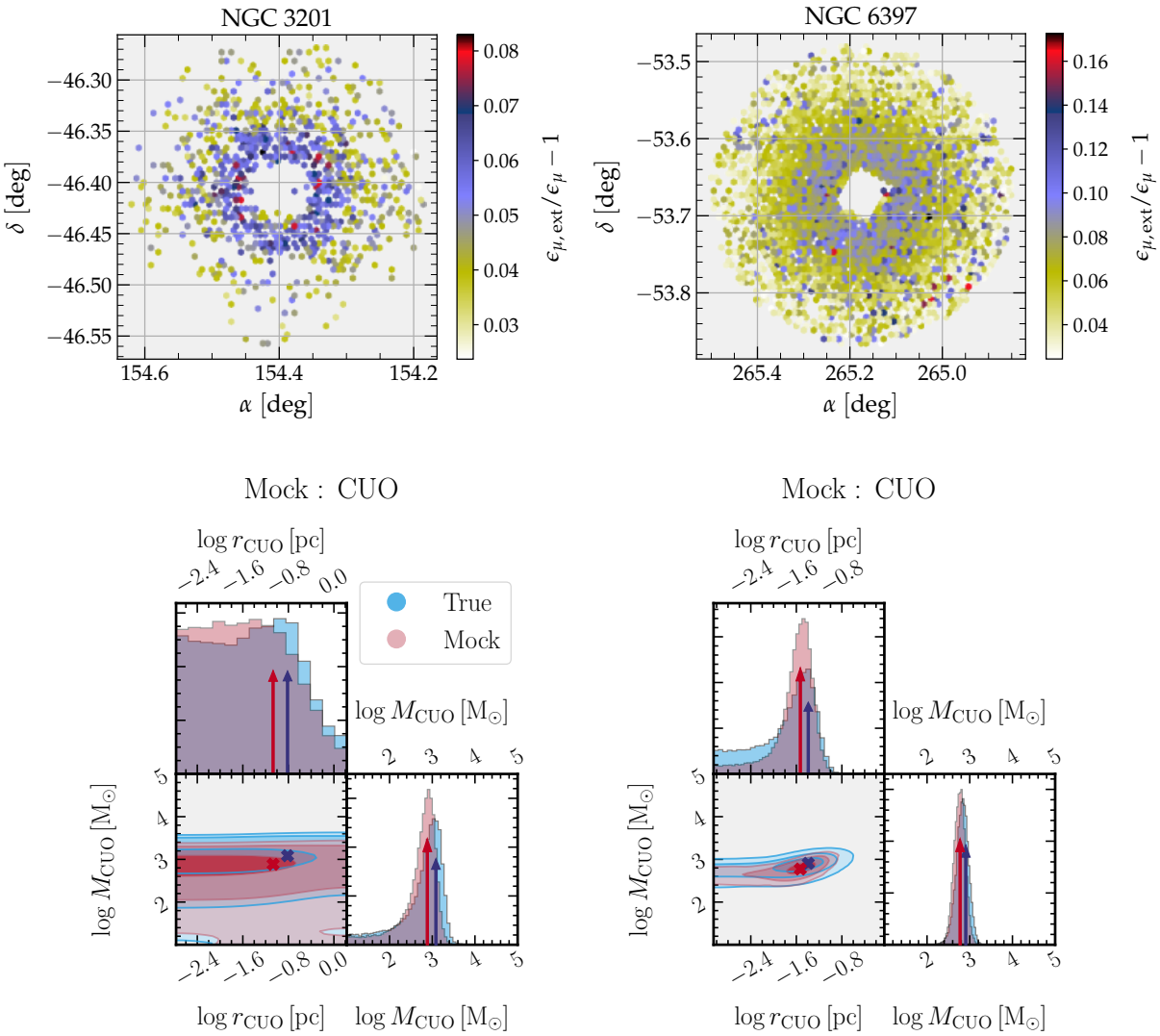

Figure B6. *Gaia systematics:* The **upper** plots evaluate the *Gaia* systematics in our cleaned *Gaia* data, computed according to eq. 3 from Vasiliev & Baumgardt (2021), using the values from their table 1 (first line, with $\epsilon_{\mu,\mathrm{sys}} = 0.026$ mas yr^{-1}). The bulk of the stars, quantified by the 84th percentile, have underestimated proper motion errors (i.e., $\epsilon_{\mu,\mathrm{ext}}/\epsilon_\mu - 1$) by only $< 6\%$ for NGC 3201 and $< 10\%$ for NGC 6397. The respective medians (50th percentile) are of 5% and 7% for NGC 3201 and NGC 6397. The **lower** plots display the comparison of marginal distributions of our standard fits (*blue*) on real data (neglecting the *Gaia* systematics) and the fits of mock data (*red*) with a sub-cluster of unseen objects, constructed according to Section 4.2, but with *Gaia* underestimated errors following the same pattern than evaluated above. One sees that the small magnitude of these *Gaia* systematics do not significantly affect our fits of both mass and extent of the inner dark population. This gives us a reasonable marge to neglect these systematics in our modelling. Furthermore, their individual, separate effects on $\epsilon_{\mu\alpha}$, $\epsilon_{\mu\delta}$ and $\rho_{\mu\alpha\delta}$, which we use in our Jeans modelling, are not yet well quantified, and assuming the same factor for all these components could insert new systematics, which in turn are beyond the scope of our modelling.

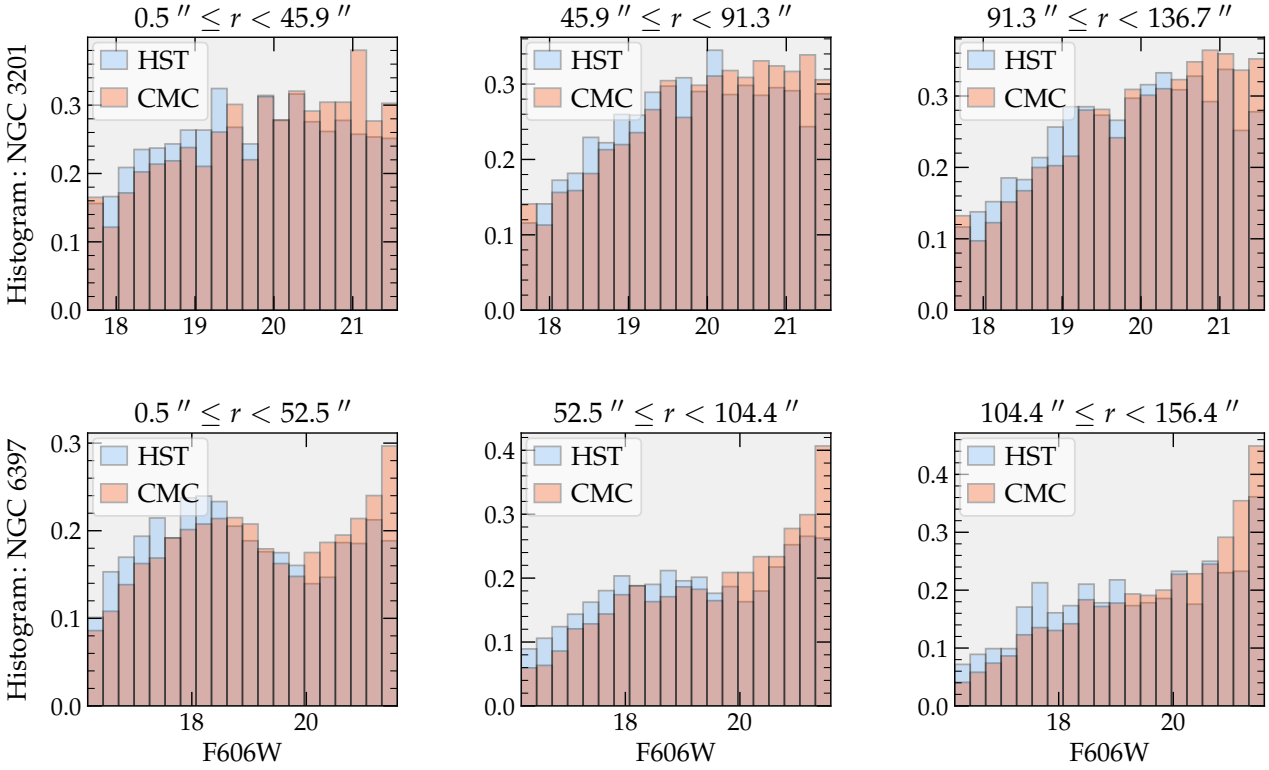

Figure B7. *Magnitude distribution:* **Normalised** histogram of CMC F606W magnitudes (orange, converted from masses with the PARSEC isochrones) and *HST* F606W magnitudes (blue), for three annuli surrounding the cluster's centre. The upper row indicates the results for NGC 3201, while the lower row depicts the behaviour for NGC 6397. For a fairer comparison, we used the non-cleaned *HST* subset, but still in the same mass/magnitude ranges of the clean data we actually use. We also forced spatial incompleteness, by assuming the following: (1) At the centre-most 500 pixels (20 arcsec), at F606W= 17 one is 100% complete, at F606W= 19 one has a completeness of 90% and at F606W= 21, one has 70% . (2) Between 500 and 1000 pixels (20 and 40 arcsec), at F606W= 17 one is 100% complete, at F606W= 19 one has a completeness of 100% and at F606W= 21 one has 85%. (3) At larger radii, one is always complete. This figure adds a strong reliability to the CMC models we used to compare our fits.

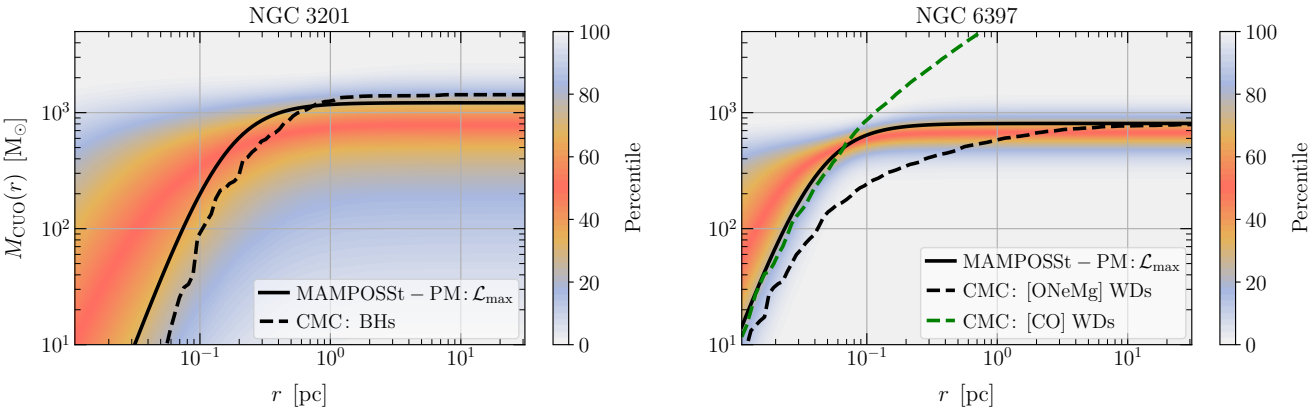

Figure B8. *Mass profiles:* Comparison of the cumulative mass profiles of the sub-clustered population of stellar remnants in NGC 3201 (*left*) and NGC 6397 (*right*), estimated by MAMPOSSt-PM (best likelihood value in **thick black**) and by CMC (**dashed black**, formed by black holes in NGC 3201 and mainly by [ONeMg] white dwarfs in NGC 6397). The colour bar indicates the percentile of the MAMPOSSt-PM MCMC chain post burn-in phase (The skewed marginal MAMPOSSt-PM mass distribution of the CUO in NGC 3201 leads to a higher mode than the median, much in line with the maximum likelihood; on the other hand, the marginal MAMPOSSt-PM mass distribution of the NGC 6397 CUO is symmetric, and the maximum likelihood value is higher than the mode). For NGC 6397, we also display the population of [CO] white dwarfs in **dashed green**, which are actually segregated deeper in the cluster's gravitational potential (as our MAMPOSSt-PM fits suggest), but ends up mixing with the luminous stellar population (hence, not forming a sub-cluster).